EUROPEAN ORGANIZATION FOR NUCLEAR RESEARCH

Search for Lepton Flavour Number violating Z^0-Decays

DELPHI Collaboration

Abstract

A search for lepton flavour number violating Z^0 decays in the channels

$$Z^0 \to \mu\tau,$$
$$Z^0 \to e\tau,$$
$$Z^0 \to e\mu,$$

using the DELPHI detector with data collected during the 1991–94 LEP runs, is described. No signal was found. Upper limits at 95% confidence level for the respective branching fractions of 1.2×10^{-5}, 2.2×10^{-5}, and 0.25×10^{-5}, were obtained.

P.Abreu[21], W.Adam[50], T.Adye[37], I.Ajinenko[42], G.D.Alekseev[16], R.Alemany[49], P.P.Allport[22], S.Almehed[24], U.Amaldi[9], S.Amato[47], A.Andreazza[28], M.L.Andrieux[14], P.Antilogus[9], W-D.Apel[17], B.Åsman[44], J-E.Augustin[25], A.Augustinus[9], P.Baillon[9], P.Bambade[19], F.Barao[21], R.Barate[14], M.Barbi[47], D.Y.Bardin[16], A.Baroncelli[40], O.Barring[24], J.A.Barrio[26], W.Bartl[50], M.J.Bates[37], M.Battaglia[15], M.Baubillier[23], J.Baudot[39], K-H.Becks[52], M.Begalli[6], P.Beilliere[8], Yu.Belokopytov[9,53], K.Belous[42], A.C.Benvenuti[5], M.Berggren[47], D.Bertini[25], D.Bertrand[2], M.Besancon[39], F.Bianchi[45], M.Bigi[45], M.S.Bilenky[16], P.Billoir[23], M-A.Bizouard[19], D.Bloch[10], M.Blume[52], T.Bolognese[39], M.Bonesini[28], W.Bonivento[28], P.S.L.Booth[22], C.Bosio[40], O.Botner[48], E.Boudinov[31], B.Bouquet[19], C.Bourdarios[9], T.J.V.Bowcock[22], M.Bozzo[13], P.Branchini[40], K.D.Brand[36], T.Brenke[52], R.A.Brenner[15], C.Bricman[2], R.C.A.Brown[9], P.Bruckman[18], J-M.Brunet[8], L.Bugge[33], T.Buran[33], T.Burgsmueller[52], P.Buschmann[52], A.Buys[9], S.Cabrera[49], M.Caccia[28], M.Calvi[28], A.J.Camacho Rozas[41], T.Camporesi[9], V.Canale[38], M.Canepa[13], K.Cankocak[44], F.Cao[2], F.Carena[9], L.Carroll[22], C.Caso[13], M.V.Castillo Gimenez[49], A.Cattai[9], F.R.Cavallo[5], V.Chabaud[9], Ph.Charpentier[9], L.Chaussard[25], P.Checchia[36], G.A.Chelkov[16], M.Chen[2], R.Chierici[45], P.Chliapnikov[42], P.Chochula[7], V.Chorowicz[9], J.Chudoba[30], V.Cindro[43], P.Collins[9], R.Contri[13], E.Cortina[49], G.Cosme[19], F.Cossutti[46], J-H.Cowell[22], H.B.Crawley[1], D.Crennell[37], G.Crosetti[13], J.Cuevas Maestro[34], S.Czellar[15], E.Dahl-Jensen[29], J.Dahm[52], B.Dalmagne[19], M.Dam[29], G.Damgaard[29], P.D.Dauncey[37], M.Davenport[9], W.Da Silva[23], C.Defoix[8], A.Deghorain[2], G.Della Ricca[46], P.Delpierre[27], N.Demaria[35], A.De Angelis[9], W.De Boer[17], S.De Brabandere[2], C.De Clercq[2], C.De La Vaissiere[23], B.De Lotto[46], A.De Min[36], L.De Paula[47], C.De Saint-Jean[39], H.Dijkstra[9], L.Di Ciaccio[38], A.Di Diodato[38], F.Djama[10], J.Dolbeau[8], M.Donszelmann[9], K.Doroba[51], M.Dracos[10], J.Drees[52], K.-A.Drees[52], M.Dris[32], J-D.Durand[25], D.Edsall[1], R.Ehret[17], G.Eigen[4], T.Ekelof[48], G.Ekspong[44], M.Elsing[52], J-P.Engel[10], B.Erzen[43], E.Falk[24], D.Fassouliotis[32], M.Feindt[9], A.Ferrer[49], S.Fichet[23], T.A.Filippas[32], A.Firestone[1], P.-A.Fischer[10], H.Foeth[9], E.Fokitis[32], F.Fontanelli[13], F.Formenti[9], B.Franek[37], P.Frenkiel[8], D.C.Fries[17], A.G.Frodesen[4], R.Fruhwirth[50], F.Fulda-Quenzer[19], J.Fuster[49], A.Galloni[22], D.Gamba[45], M.Gandelman[47], C.Garcia[49], J.Garcia[41], C.Gaspar[9], U.Gasparini[36], Ph.Gavillet[9], E.N.Gazis[32], D.Gele[10], J-P.Gerber[10], R.Gokieli[51], B.Golob[43], G.Gopal[37], L.Gorn[1], M.Gorski[51], Yu.Gouz[45,53], V.Gracco[13], E.Graziani[40], C.Green[22], A.Grefrath[52], P.Gris[39], G.Grosdidier[19], K.Grzelak[51], S.Gumenyuk[28,53], P.Gunnarsson[44], M.Gunther[48], J.Guy[37], F.Hahn[9], S.Hahn[52], Z.Hajduk[18], A.Hallgren[48], K.Hamacher[52], J.Hansen[33], F.J.Harris[35], V.Hedberg[24], R.Henriques[21], J.J.Hernandez[49], P.Herquet[2], H.Herr[9], T.L.Hessing[35], E.Higon[49], H.J.Hilke[9], T.S.Hill[1], S-O.Holmgren[44], P.J.Holt[35], D.Holthuizen[31], S.Hoorelbeke[2], M.Houlden[22], J.Hrubec[50], K.Huet[2], K.Hultqvist[44], J.N.Jackson[22], R.Jacobsson[44], P.Jalocha[18], R.Janik[7], Ch.Jarlskog[24], G.Jarlskog[24], P.Jarry[39], B.Jean-Marie[19], E.K.Johansson[44], L.Jonsson[24], P.Jonsson[24], C.Joram[9], P.Juillot[10], M.Kaiser[17], F.Kapusta[23], K.Karafasoulis[11], M.Karlsson[44], E.Karvelas[11], S.Katsanevas[3], E.C.Katsoufis[32], R.Keranen[4], Yu.Khokhlov[42], B.A.Khomenko[16], N.N.Khovanski[16], B.King[22], N.J.Kjaer[31], O.Klapp[52], H.Klein[9], A.Klovning[4], P.Kluit[31], B.Koene[31], P.Kokkinias[11], M.Koratzinos[9], K.Korcyl[18], V.Kostioukhine[42], C.Kourkoumelis[3], O.Kouznetsov[13,16], M.Krammer[50], C.Kreuter[17], I.Kronkvist[24], Z.Krumstein[16], W.Krupinski[18], P.Kubinec[7], W.Kucewicz[18], K.Kurvinen[15], C.Lacasta[49], I.Laktineh[25], J.W.Lamsa[1], L.Lanceri[46], D.W.Lane[1], P.Langefeld[52], V.Lapin[42], J-P.Laugier[39], R.Lauhakangas[15], G.Leder[50], F.Ledroit[14], V.Lefebure[2], C.K.Legan[1], R.Leitner[30], J.Lemonne[2], G.Lenzen[52], V.Lepeltier[19], T.Lesiak[18], J.Libby[35], D.Liko[50], R.Lindner[52], A.Lipniacka[44], I.Lippi[36], B.Loerstad[24], J.G.Loken[35], J.M.Lopez[41], D.Loukas[11], P.Lutz[39], L.Lyons[35], J.MacNaughton[50], G.Maehlum[17], J.R.Mahon[6], A.Maio[21], T.G.M.Malmgren[44], V.Malychev[16], F.Mandl[50], J.Marco[41], R.Marco[41], B.Marechal[47], M.Margoni[36], J-C.Marin[9], C.Mariotti[40], A.Markou[11], C.Martinez-Rivero[41], F.Martinez-Vidal[49], S.Marti i Garcia[22], J.Masik[30], F.Matorras[41], C.Matteuzzi[28], G.Matthiae[38], M.Mazzucato[36], M.Mc Cubbin[9], R.Mc Kay[1], R.Mc Nulty[22], J.Medbo[48], M.Merk[31], C.Meroni[28], S.Meyer[17], W.T.Meyer[1], M.Michelotto[36], E.Migliore[45], L.Mirabito[25], W.A.Mitaroff[50], U.Mjoernmark[24], T.Moa[44], R.Moeller[29], K.Moenig[9], M.R.Monge[13], P.Morettini[13], H.Mueller[17], K.Muenich[52], M.Mulders[31], L.M.Mundim[6], W.J.Murray[37], B.Muryn[18], G.Myatt[35], F.Naraghi[14], F.L.Navarria[5], S.Navas[49], K.Nawrocki[51], P.Negri[28], W.Neumann[52], N.Neumeister[50], R.Nicolaidou[3], B.S.Nielsen[29], M.Nieuwenhuizen[31], V.Nikolaenko[10], P.Niss[44], A.Nomerotski[36], A.Normand[35], M.Novak[12], W.Oberschulte-Beckmann[17], V.Obraztsov[42], A.G.Olshevski[16], A.Onofre[21], R.Orava[15], K.Osterberg[15], A.Ouraou[39], P.Paganini[19], M.Paganoni[9,28], P.Pages[10], R.Pain[23], H.Palka[18], Th.D.Papadopoulou[32], K.Papageorgiou[11], L.Pape[9], C.Parkes[35], F.Parodi[13], A.Passeri[40], M.Pegoraro[36], L.Peralta[21], H.Pernegger[50], A.Perrotta[5], C.Petridou[46], A.Petrolini[13], M.Petrovyck[42], H.T.Phillips[37], G.Piana[13], F.Pierre[39], M.Pimenta[21], O.Podobrin[17], M.E.Pol[6], G.Polok[18], P.Poropat[46], V.Pozdniakov[16], P.Privitera[38], N.Pukhaeva[16], A.Pullia[28], D.Radojicic[35], S.Ragazzi[28], H.Rahmani[32], P.N.Ratoff[20], A.L.Read[33], M.Reale[52], P.Rebecchi[19], N.G.Redaelli[28], M.Regler[50], D.Reid[9], P.B.Renton[35], L.K.Resvanis[3], F.Richard[19], J.Richardson[22], J.Ridky[12], G.Rinaudo[45], I.Ripp[39], A.Romero[45], I.Roncagliolo[13], P.Ronchese[36], L.Roos[14], E.I.Rosenberg[1], E.Rosso[9], P.Roudeau[19], T.Rovelli[5], W.Ruckstuhl[31], V.Ruhlmann-Kleider[39], A.Ruiz[41], K.Rybicki[18], H.Saarikko[15], Y.Sacquin[39], A.Sadovsky[16], O.Sahr[14], G.Sajot[14], J.Salt[49], J.Sanchez[26], M.Sannino[13], M.Schimmelpfennig[17], H.Schneider[17], U.Schwickerath[17], M.A.E.Schyns[52], G.Sciolla[45], F.Scuri[46], P.Seager[20], Y.Sedykh[16], A.M.Segar[35], A.Seitz[17], R.Sekulin[37], L.Serbelloni[38], R.C.Shellard[6], P.Siegrist[39], R.Silvestre[39], S.Simonetti[39], F.Simonetto[36], A.N.Sisakian[16], B.Sitar[7], T.B.Skaali[33], G.Smadja[25], N.Smirnov[42], O.Smirnova[24], G.R.Smith[37], A.Sokolov[42], R.Sosnowski[51], D.Souza-Santos[6], T.Spassov[21], E.Spiriti[40], P.Sponholz[52], S.Squarcia[13], C.Stanescu[40], S.Stapnes[33], I.Stavitski[36], K.Stevenson[35], F.Stichelbaut[9], A.Stocchi[19], J.Strauss[50], R.Strub[10], B.Stugu[4], M.Szczekowski[51], M.Szeptycka[51], T.Tabarelli[28], J.P.Tavernet[23], E.Tcherniaev[42],

O.Tchikilev[42], J.Thomas[35], A.Tilquin[27], J.Timmermans[31], L.G.Tkatchev[16], T.Todorov[10], S.Todorova[10], D.Z.Toet[31], A.Tomaradze[2], B.Tome[21], A.Tonazzo[28], L.Tortora[40], G.Transtromer[24], D.Treille[9], W.Trischuk[9], G.Tristram[8], A.Trombini[19], C.Troncon[28], A.Tsirou[9], M-L.Turluer[39], I.A.Tyapkin[16], M.Tyndel[37], S.Tzamarias[22], B.Ueberschaer[52], O.Ullaland[9], V.Uvarov[42], G.Valenti[5], E.Vallazza[9], G.W.Van Apeldoorn[31], P.Van Dam[31], W.K.Van Doninck[2], J.Van Eldik[31], A.Van Lysebetten[2], N.Vassilopoulos[35], G.Vegni[28], L.Ventura[36], W.Venus[37], F.Verbeure[2], M.Verlato[36], L.S.Vertogradov[16], D.Vilanova[39], P.Vincent[25], L.Vitale[46], E.Vlasov[42], A.S.Vodopyanov[16], V.Vrba[12], H.Wahlen[52], C.Walck[44], F.Waldner[46], M.Weierstall[52], P.Weilhammer[9], C.Weiser[17], A.M.Wetherell[9], D.Wicke[52], J.H.Wickens[2], M.Wielers[17], G.R.Wilkinson[35], W.S.C.Williams[35], M.Winter[10], M.Witek[18], T.Wlodek[19], K.Woschnagg[48], K.Yip[35], O.Yushchenko[42], F.Zach[25], A.Zaitsev[42], A.Zalewska[9], P.Zalewski[51], D.Zavrtanik[43], E.Zevgolatakos[11], N.I.Zimin[16], M.Zito[39], D.Zontar[43], G.C.Zucchelli[44], G.Zumerle[36]

[1]Department of Physics and Astronomy, Iowa State University, Ames IA 50011-3160, USA
[2]Physics Department, Univ. Instelling Antwerpen, Universiteitsplein 1, B-2610 Wilrijk, Belgium
    and IIHE, ULB-VUB, Pleinlaan 2, B-1050 Brussels, Belgium
    and Faculté des Sciences, Univ. de l'Etat Mons, Av. Maistriau 19, B-7000 Mons, Belgium
[3]Physics Laboratory, University of Athens, Solonos Str. 104, GR-10680 Athens, Greece
[4]Department of Physics, University of Bergen, Allégaten 55, N-5007 Bergen, Norway
[5]Dipartimento di Fisica, Università di Bologna and INFN, Via Irnerio 46, I-40126 Bologna, Italy
[6]Centro Brasileiro de Pesquisas Físicas, rua Xavier Sigaud 150, RJ-22290 Rio de Janeiro, Brazil
    and Depto. de Física, Pont. Univ. Católica, C.P. 38071 RJ-22453 Rio de Janeiro, Brazil
    and Inst. de Física, Univ. Estadual do Rio de Janeiro, rua São Francisco Xavier 524, Rio de Janeiro, Brazil
[7]Comenius University, Faculty of Mathematics and Physics, Mlynska Dolina, SK-84215 Bratislava, Slovakia
[8]Collège de France, Lab. de Physique Corpusculaire, IN2P3-CNRS, F-75231 Paris Cedex 05, France
[9]CERN, CH-1211 Geneva 23, Switzerland
[10]Centre de Recherche Nucléaire, IN2P3 - CNRS/ULP - BP20, F-67037 Strasbourg Cedex, France
[11]Institute of Nuclear Physics, N.C.S.R. Demokritos, P.O. Box 60228, GR-15310 Athens, Greece
[12]FZU, Inst. of Physics of the C.A.S. High Energy Physics Division, Na Slovance 2, 180 40, Praha 8, Czech Republic
[13]Dipartimento di Fisica, Università di Genova and INFN, Via Dodecaneso 33, I-16146 Genova, Italy
[14]Institut des Sciences Nucléaires, IN2P3-CNRS, Université de Grenoble 1, F-38026 Grenoble Cedex, France
[15]Research Institute for High Energy Physics, SEFT, P.O. Box 9, FIN-00014 Helsinki, Finland
[16]Joint Institute for Nuclear Research, Dubna, Head Post Office, P.O. Box 79, 101 000 Moscow, Russian Federation
[17]Institut für Experimentelle Kernphysik, Universität Karlsruhe, Postfach 6980, D-76128 Karlsruhe, Germany
[18]Institute of Nuclear Physics and University of Mining and Metalurgy, Ul. Kawiory 26a, PL-30055 Krakow, Poland
[19]Université de Paris-Sud, Lab. de l'Accélérateur Linéaire, IN2P3-CNRS, Bât. 200, F-91405 Orsay Cedex, France
[20]School of Physics and Chemistry, University of Lancaster, Lancaster LA1 4YB, UK
[21]LIP, IST, FCUL - Av. Elias Garcia, 14-1°, P-1000 Lisboa Codex, Portugal
[22]Department of Physics, University of Liverpool, P.O. Box 147, Liverpool L69 3BX, UK
[23]LPNHE, IN2P3-CNRS, Universités Paris VI et VII, Tour 33 (RdC), 4 place Jussieu, F-75252 Paris Cedex 05, France
[24]Department of Physics, University of Lund, Sölvegatan 14, S-22363 Lund, Sweden
[25]Université Claude Bernard de Lyon, IPNL, IN2P3-CNRS, F-69622 Villeurbanne Cedex, France
[26]Universidad Complutense, Avda. Complutense s/n, E-28040 Madrid, Spain
[27]Univ. d'Aix - Marseille II - CPP, IN2P3-CNRS, F-13288 Marseille Cedex 09, France
[28]Dipartimento di Fisica, Università di Milano and INFN, Via Celoria 16, I-20133 Milan, Italy
[29]Niels Bohr Institute, Blegdamsvej 17, DK-2100 Copenhagen 0, Denmark
[30]NC, Nuclear Centre of MFF, Charles University, Areal MFF, V Holesovickach 2, 180 00, Praha 8, Czech Republic
[31]NIKHEF, Postbus 41882, NL-1009 DB Amsterdam, The Netherlands
[32]National Technical University, Physics Department, Zografou Campus, GR-15773 Athens, Greece
[33]Physics Department, University of Oslo, Blindern, N-1000 Oslo 3, Norway
[34]Dpto. Fisica, Univ. Oviedo, C/P. Pérez Casas, S/N-33006 Oviedo, Spain
[35]Department of Physics, University of Oxford, Keble Road, Oxford OX1 3RH, UK
[36]Dipartimento di Fisica, Università di Padova and INFN, Via Marzolo 8, I-35131 Padua, Italy
[37]Rutherford Appleton Laboratory, Chilton, Didcot OX11 OQX, UK
[38]Dipartimento di Fisica, Università di Roma II and INFN, Tor Vergata, I-00173 Rome, Italy
[39]CEA, DAPNIA/Service de Physique des Particules, CE-Saclay, F-91191 Gif-sur-Yvette Cedex, France
[40]Istituto Superiore di Sanità, Ist. Naz. di Fisica Nucl. (INFN), Viale Regina Elena 299, I-00161 Rome, Italy
[41]Instituto de Fisica de Cantabria (CSIC-UC), Avda. los Castros, S/N-39006 Santander, Spain, (CICYT-AEN93-0832)
[42]Inst. for High Energy Physics, Serpukov P.O. Box 35, Protvino, (Moscow Region), Russian Federation
[43]J. Stefan Institute and Department of Physics, University of Ljubljana, Jamova 39, SI-61000 Ljubljana, Slovenia
[44]Fysikum, Stockholm University, Box 6730, S-113 85 Stockholm, Sweden
[45]Dipartimento di Fisica Sperimentale, Università di Torino and INFN, Via P. Giuria 1, I-10125 Turin, Italy
[46]Dipartimento di Fisica, Università di Trieste and INFN, Via A. Valerio 2, I-34127 Trieste, Italy
    and Istituto di Fisica, Università di Udine, I-33100 Udine, Italy
[47]Univ. Federal do Rio de Janeiro, C.P. 68528 Cidade Univ., Ilha do Fundão BR-21945-970 Rio de Janeiro, Brazil
[48]Department of Radiation Sciences, University of Uppsala, P.O. Box 535, S-751 21 Uppsala, Sweden
[49]IFIC, Valencia-CSIC, and D.F.A.M.N., U. de Valencia, Avda. Dr. Moliner 50, E-46100 Burjassot (Valencia), Spain
[50]Institut für Hochenergiephysik, Österr. Akad. d. Wissensch., Nikolsdorfergasse 18, A-1050 Vienna, Austria
[51]Inst. Nuclear Studies and University of Warsaw, Ul. Hoza 69, PL-00681 Warsaw, Poland
[52]Fachbereich Physik, University of Wuppertal, Postfach 100 127, D-42097 Wuppertal, Germany
[53]On leave of absence from IHEP Serpukhov

1 Introduction

The standard model (SM) does not contain first order flavour changing neutral currents. However, several extensions to it allow flavour changing neutral currents with predicted branching ratios of lepton flavour number violating Z^0 decays ranging from $\sim 10^{-4}$ to $\sim 10^{-9}$ [1]–[8]. Thus lepton flavour violation constitutes an important potential signal of physics beyond the SM. While the branching ratio of $Z^0 \to e\mu$ can be concluded to be below 10^{-12} from the absence of $\mu \to eee$ decays, the absence of neutrinoless $\tau \to \mu\mu\mu$, $\mu\mu e$, μee, and eee decays only imposes constraints that $Z^0 \to \mu\tau$, $e\tau$ be below a few times 10^{-4} [9]. In models with momentum transfer dependent form factors, the low energy limits may not be valid. For a recent review of lepton flavour violation physics, see ref. [10].

In this letter a search for Z^0 decays to $\mu\tau$, $e\tau$, and $e\mu$ with the DELPHI detector is described. A previous DELPHI search based on data from 1990 and 1991 is reported in ref. [11]. Previous searches have also been reported by the other LEP experiments [12–14].The most stringent published limits, ref. [12], are $B(Z^0 \to \mu\tau) < 1.7 \times 10^{-5}$, $B(Z^0 \to e\tau) < 0.98 \times 10^{-5}$, and $B(Z^0 \to e\mu) < 0.17 \times 10^{-5}$, at 95% confidence level.

2 The detector

Since the quality of the three analyses described depends crucially on the momentum resolution, which deteriorates at small scattering angles, only the barrel part of the DELPHI detector was used in the three analyses. The barrel definition depended on the channel studied, and are given in the detailed description of each analysis in the following sections. A complete description of the DELPHI detector can be found in [15]. Here only the parts relevant to this study will be mentioned. The main tracking device was the Time Projection Chamber (TPC), extending radially from 32 to 116 cm and from -135 cm to $+135$ cm in z (position along the beam), covering approximately a polar angle (θ) range from 20° to 160°. In addition to providing precise track points, the specific ionization, dE/dx, was used for particle identification. The TPC tracking was supplemented by precise $R\Phi$ information from the Vertex Detector (VD) (three layers at radii between 6 and 11 cm). Here R is the radial coordinate in a plane perpendicular to the beam axis, and Φ the azimuthal angle around the beam. Additional space information came from the Inner Detector drift chamber (ID), positioned between the VD and the TPC, and from the Outer Detector (OD), a five layer drift tube detector at radii from 198 to 206 cm for a polar angle range from 43° to 137°. A momentum resolution of $\sim 4\%$ was measured with muon pairs at 45 GeV/c.

Electromagnetic calorimetry was provided by the High density Projection Chamber (HPC), a lead/gas calorimeter with the ionization electrons drifting in the gas gaps to multiwire proportional chambers. The detector gave 3-dimensional charge distributions in nine radial samplings over 18 radiation lengths with a $\Delta z \Delta \Phi$ granularity of about 4 mm×1°. The polar angular coverage was 43° to 137°. An energy resolution of $\sim 6\%$ was measured with electrons of 45 GeV.

Hadronic calorimetry was provided by the Hadron Calorimeter (HCAL), a 20 gap limited streamer/iron plate detector, read out in four radial layers with a granularity of about 3×3 degrees in θ and Φ.

Muons penetrating the iron of the HCAL were detected by the Barrel Muon chambers (MUB), providing three dimensional track points for polar angles between 52° and 128°.

Towards the end of the data taking, the barrel muon chamber coverage was extended to 42° (138°).

In the three analyses reported here, the particle identification was based on the calorimetry, the dE/dx measurements, and the muon chamber hit patterns.

3 Method

A search for rare processes is sensitive to detector malfunctions. Therefore strict detector quality requirements were applied, and known dead detector zones were masked off. Data from the years 1991–1994 passing the detector quality cuts amounted to an integrated luminosity of approximately 100 pb^{-1}, corresponding to about 3.9×10^6 Z^0's, the numbers being slightly different for the three channels due to different detector quality cuts. This corresponds to ~85% of the total integrated luminosity. The $\mu\tau$ ($e\tau$) search looked for a high energy muon (electron) recoiling against a low multiplicity system with the leading charged particle being different from a muon (electron), *i.e.* τ decays to $\mu\nu\bar{\nu}$ ($e\nu\bar{\nu}$) were not accepted. The events were divided into two hemispheres by a plane through the origin perpendicular to the thrust axis. The $e\mu$ analysis looked for events with a high energy electron in one hemisphere and a high momentum muon in the other hemisphere. Efficiencies and backgrounds were determined partly from data, and partly from Bhabha [16], dimuon [17], and τ-pair [18] simulated event samples with detector response functions simulated [19] and adjusted to fit real data. For the generation of signals, modified versions of KORALZ [18] were used. The modifications consisted of renaming one or both τ to e or μ as appropriate, and suppressing the τ decay for the renamed lepton(s). Also the generated signal events were passed through the detector response simulation.

In the absence of a signal, upper limits were determined. In the $\mu\tau$ ($e\tau$) case, an unbinned likelihood method was applied. The likelihood function was defined as

$$L = \prod_{i=1}^{N_{data}} \left(f_b P_b(x_i) + f_s P_s(x_i) \right) \tag{1}$$

where x_i is the muon momentum (electron energy) normalized to the beam energy, f_s and f_b are the signal and background fractions in the data, and $P_b(x)$ and $P_s(x)$ the normalized probability densities for the background and signal respectively, as determined from simulation. The background fraction is $f_b = 1 - f_s$. The signal fraction was parametrized as $f_s = \frac{B\xi}{N_{data}}$ where B is the signal branching fraction and N_{data} the number of accepted candidates in data. The sensitivity factor ξ is given by the sum over the four years of data taking of the efficiency corrected number of Z^0's, $\epsilon_y N_Z^y$, where ϵ_y is the 4π efficiency of the event selection for year y. N_Z^y was calculated as a sum over the LEP energy points from the total cross sections and the corresponding luminosities. The likelihood function for the $\mu\tau$ ($e\tau$) channel is sensitive to the amount of muon pair (electron pair) background, which peaks in the signal region. The systematic errors arising from the uncertainties in these background channels were accounted for by applying a likelihood profile technique, *i.e.* the likelihood function which was studied, was maximized with respect to the number of expected muon pair (electron pair) events, which was treated as a free parameter with a Gaussian probability density.

The 95% signal branching fraction upper limits were derived by finding the 95% point of the area under the profile likelihood function as a function of the signal branching fraction. This corresponds to a Bayesian approach with a uniform prior probability

density [20]. The systematic error in the sensitivity factor was conservatively accounted for [21] by subtracting one sigma from the sensitivity factor.

In the $e\mu$ case, zero events passed the analysis, and the upper limit was determined by Poisson statistics. In this case the systematic error in the sensitivity factor was accounted for by the method of ref. [21].

4   Event selection

4.1   Leptonic preselection

The first step of the three analyses consisted of a common leptonic event preselection. The number of reconstructed charged particles with minimum distance to the interaction point of less than 1.5 cm in radius and less than 4.5 cm in the projection along the beam was required to be $2 \leq N_{track} \leq 6$. There had to be at least one track in each hemisphere. The visible energy, defined as the sum of charged track momenta plus unassociated electromagnetic energy, was required to be greater than 8 GeV. The isolation angle, the smallest angle between tracks in the two opposite hemispheres, was required to be greater than 160°. Events accepted by the leptonic preselection were passed on to the event selections as described in the following sections.

4.2   The $\mu\tau$ search

The track of the leading charged particle in each hemisphere was required to point to the region with full barrel muon chamber coverage, *i.e.* to have $52° < \theta < 128°$. Cosmic radiation events were suppressed by cuts on the impact point of the leading charged particle in each hemisphere in the radial and in the z-coordinate of $R_{imp} < 1$ cm, $|z_{imp}| < 4$ cm, and $|\Delta z_{imp}| < 1$ cm where Δz_{imp} denotes the difference between the leading charged particle in the two hemispheres. The analysis proceeded by searching for a high momentum ($p/E_{beam} > 0.3$) muon in one of the hemispheres. If one was found, strict cuts were applied to the leading charged particle in the opposite hemisphere to reject muons.

The muon identification required the HCAL response to be compatible with a minimum ionizing particle by demanding that E_{lay}^{HCAL}(mips), the HCAL energy per fired layer normalized to the mean minimum ionizing particle (mip) response, fulfilled $0 < E_{lay}^{HCAL}$(mips)< 3.5. Furthermore at least one MUB hit associated to the track was required. In addition, non-zero energy in the fourth HCAL layer was required, suppressing background from misidentified hadrons. Only one charged particle in the muon hemisphere was accepted. The track was required to have the chi-squared per degree of freedom from the track fit less than 5, and tracks with a particle momentum greater than 130% of the beam energy were rejected to avoid background due to badly reconstructed tracks. Muon momentum spectra from data and Monte Carlo simulations are shown in Fig. 1 a).

The muon veto selection in the opposite hemisphere required the combined HPC and HCAL response of the leading charged particle to be incompatible with a muon. If there was non-zero HCAL energy associated to the track in any of layers 2 through 4, the track was rejected if the HCAL response was in the mip peak. If there was zero HCAL energy in layers 2 through 4, but the response in the first layer was in the mip peak, then the track was rejected if the electromagnetic energy divided by the momentum was not compatible with an electron, *i.e.* if $E_{em}/p < 0.5$ or $E_{em}/p > 1.5$, where E_{em} denotes electromagnetic energy associated to the track. If there was zero HCAL energy associated to the track, it

was expected to be an electron, and the associated electromagnetic energy was required to be greater than 0.5 GeV. To suppress muons further, the track was rejected if it had one or more associated muon chamber hits or if it had non-zero associated HCAL energy in the fourth HCAL layer. Furthermore, to be sure a possible muon would have reached the muon chambers, the momentum was required to be larger than 2.5 GeV/c. To ensure high MUB efficiency, angular cuts were applied to eliminate zones with poor muon chamber coverage. In the case of more than one charged particle in the hemisphere, all were required to be seen by the VD, thus minimizing the chance of having an electron from a photon conversion as the leading charged particle.

To suppress muon pair background further, the event was required to have an acollinearity greater than 0.1°. The radial momentum, defined as $p_{rad} = \sqrt{p_1^2 + p_2^2}$ where p_i is the leading charged particle momentum in hemisphere i, was required to satisfy $p_{rad} < 62$ GeV/c. The p_{rad} distributions for muon pairs, the $\mu\tau$ signal, and tau pairs are shown in Fig. 1 b). Finally, the leading charged particles in the two hemispheres were required to have opposite charges.

The number of $\mu\tau$ event candidates selected by these cuts was 4137.

4.3   The $e\tau$ search

The track of the leading charged particle in each hemisphere was required to point to the region with full barrel electromagnetic calorimeter coverage, *i.e.* to have $45° < \theta < 135°$. After cuts to reduce background from cosmic radiation events similar to those described in section 4.2, the analysis proceeded by searching for a high energy electron ($E_{em}/E_{beam} > 0.3$) in one of the hemispheres. If one was found, strict cuts were applied to the leading charged particle in the opposite hemisphere to reject electrons.

In addition to the high electromagnetic energy requirement, the electron identification required the electromagnetic energy divided by the momentum measured from track curvature, E_{em}/p, to be consistent with electron response by demanding $0.6 < E_{em}/p < 1.5$. The E_{em}/p distributions for real and simulated data are shown in Fig. 2 a). Hadronic and radiative muon backgrounds were suppressed by rejecting the candidate if it had non-zero associated HCAL energy in any of layers 2 through 4, or if it had one or more associated muon chamber hits. Candidates with an associated electromagnetic energy greater than 130% of the beam energy were rejected to avoid fake electron candidates from noisy HPC channels. Finally, cuts on the longitudinal pattern of the HPC energy deposits and on dE/dx from the TPC were imposed to suppress background from misidentified hadrons.

The electron veto selection in the opposite hemisphere first applied angular cuts to eliminate dead or weak zones in the electromagnetic calorimeter. If the non-electron candidate had more than 2.5 times the average mip response in the sum of HCAL layers 2 through 4, the event was then passed on to the last step of the analysis in which cuts were made in variables for the whole event, involving both hemispheres. If not, the non-electron candidate was subjected to the following cuts. The electromagnetic energy divided by the momentum had to be inconsistent with the expected electron response. For particles below 8 GeV/c the TPC dE/dx response was required to be inconsistent with that of an electron. Particles above 8 GeV/c were required to have nonzero associated energy in any of HCAL layers 2 through 4 or at least one associated muon chamber hit.

Finally, the surviving events had to satisfy the following two criteria involving both hemispheres: the acollinearity angle had to be greater than 0.3°, and the radial electromagnetic energy, E_{rad}, had to be smaller than 59 GeV. The radial electromagnetic energy

was defined as $E_{rad} = \sqrt{(E^1_{em})^2 + (E^2_{em})^2}$ where E^i_{em} denotes the associated electromagnetic energy of the leading charged particle in hemisphere i. The E_{rad} distributions for simulated Bhabha events, tau pairs, and the $e\tau$ signal are shown in Fig. 2 b).

The number of $e\tau$ event candidates selected by these cuts was 4145.

4.4 The $e\mu$ search

The $e\mu$ signal consists of back-to-back electron-muon systems, with the energy of both leptons consistent with the beam energy. Thus cosmics as well as tau pair background are heavily suppressed in the signal region. This allows for somewhat looser selection cuts than in the previous analyses. Cosmic rays were suppressed further by requiring the tracks to have an impact parameter $R_{imp} < 1.5$ cm. The track of the leading charged particle in each hemisphere was required to point to the region with full barrel electromagnetic calorimeter coverage, $i.e.$ to have $45° < \theta < 135°$.

The analysis proceeded by searching for a muon in one hemisphere and an electron in the other one. The muon selection accepted only one charged particle in the hemisphere, which had to have at least one associated muon chamber hit and an HCAL response compatible with that of a minimum ionizing particle. The HPC energy associated to the track was required to satisfy $E_{em}/E_{beam} < 0.8$ to suppress Bhabha background. The momentum was required to be larger than 30% of the beam momentum and, to ensure good track reconstruction quality, smaller than 130% of the beam momentum.

The electron selection also accepted only one charged particle in the hemisphere. In addition to demanding $E_{em}/E_{beam} > 0.3$, the track was required to have zero energy in HCAL layers 2 through 4 and no muon chamber hits. An associated energy in the first HCAL layer of up to 2.5 times the minimum ionizing particle response was accepted to allow for leakage through the HPC. Tracks with associated electromagnetic energy or reconstructed momentum larger than 130% of the beam energy, indicating energy or track reconstruction problems, were rejected.

The number of $e\mu$ event candidates selected by these cuts was 988.

5 Efficiencies

The efficiencies of the analyses were determined as the product of the preselection efficiency ϵ_{presel}, the lepton identification efficiency $\epsilon_{ID} = \epsilon_{l1}\epsilon_{l2}$, and the correlation efficiency ϵ_{corr}. Here ϵ_{l1} (ϵ_{l2}) is the μ (τ) selection efficiency for the $\mu\tau$ analysis, the e (τ) selection efficiency for the $e\tau$ analysis, and the e (μ) selection efficiency for the $e\mu$ analysis. The preselection efficiency was determined from simulated signal event samples. The correlation efficiency included the cuts on global event variables and small hemisphere correlation effects and was determined from simulated signal samples. The lepton identification efficiencies were measured on tagged electron, muon and tau pairs in the data.

The muon pairs were tagged by requiring a muon with normalized momentum greater that $0.9 \times E_{beam}$ to be found by the muon selection routine. In addition, the muon was required to be accepted as such by DELPHI's standard muon identification [15]. In order to suppress tau pairs, the acollinearity angle of the event was required to be smaller than $0.1°$ and the visible energy was required to be greater than $1.4 \times E_{beam}$. This resulted in a sample of 35000 tagged muon pairs with negligible background from electron and tau pairs. The muon in the hemisphere opposite to the tagged one was used in the efficiency measurement.

Channel	ϵ_{presel}	ϵ_{l1}	ϵ_{l2}	ϵ_{corr}
$Z^0 \rightarrow \mu\tau$	47.1±0.4	84.5±0.2	45.0±0.2	91.9 ±0.7
$Z^0 \rightarrow e\tau$	54.5±0.5	69.1±0.2	44.9±0.5	98.3 ±0.9
$Z^0 \rightarrow e\mu$	57.5±0.4	84.6±0.2	82.8±0.1	77.4 ±0.6

Table 1: Efficiencies (%) for the three analyses. See the text. The errors are statistical only. In the $e\mu$ case, the hemisphere-correlating cuts included in ϵ_{corr} include the cuts defining the signal region (see the text and Fig. 9).

The electron pairs were tagged by requiring an electron with normalized electromagnetic energy greater that $0.9 \times E_{beam}$ to be found by the electron selection routine. In order to suppress tau pair background, the acollinearity angle of the event was required to be smaller than 0.2° and the visible energy was required to be greater than $1.4 \times E_{beam}$. This resulted in a sample of 55000 tagged electron pairs with negligible background from muon and tau pairs. The electron in the opposite hemisphere to the tagged one was used in the efficiency measurement.

The tau pairs were selected by applying the algorithm used by DELPHI's line shape analysis [22], resulting in a sample of 120000 tagged tau pairs. The electron pair background was determined on Monte Carlo generated data to be 1% and the muon pair background to be 0.5%.

Corrections due to cracks and dead detector elements were determined from simulated electron, muon, and tau pair samples and are included in the efficiencies given in table 1. In addition to the cuts described in section 4.1, the preselection efficiency included the barrel definition cut and the cuts against cosmics.

The efficiencies varied slightly between the different years due to different detector versions. The most significant effect was an increase in the $e\mu$ efficiency due to increased muon chamber coverage in the 45° region in parts of the 1994 run. The efficiencies presented in table 1 are luminosity-weighted averages over all four years, with their statistical errors.

The signal trigger efficiency is expected to be the same as the lepton pair trigger efficiencies, which are estimated to be larger than 99.9% [23]. A value of 100% was used, and a 0.1% contribution was added to the systematic error.

The systematic error had additional contributions from backgrounds in the tagged data samples and small discrepancies between simulated and real data. The systematics from background in the tagged lepton samples was conservatively estimated to be equal to the background. The effect of small differences between the real and simulated data was estimated as the difference in the efficiency as measured with and without smearing the simulated data to better resemble the real data, amounting to 1.4%. Added in quadrature and including the 0.1% contribution from the trigger efficiency, this gave a systematic uncertainty on the efficiency of 1.8%.

6   Results

The p/E_{beam} distribution for $\mu\tau$ candidates is shown in Fig. 3, for background, signal, and data. The corresponding likelihood distribution (see section 3) is shown in Fig. 4. The background was completely dominated by tau pairs. No candidates were accepted from a simulated sample of 186000 Bhabha events (the total real data sample corresponds

Channel	Efficiency-corrected number of Z^0	Branching ratio upper limit (95% confidence level)
$Z^0 \to \mu\tau$	$(645\pm15)\times10^3$	1.2×10^{-5}
$Z^0 \to e\tau$	$(630\pm16)\times10^3$	2.2×10^{-5}
$Z^0 \to e\mu$	$(1224\pm38)\times10^3$	0.25×10^{-5}

Table 2: Summary of results for the three channels. Errors include systematics.

to about 130000 Bhabha events produced), and the expected luminosity scaled muon pair background was estimated from simulations to be 5.2 events in the whole sample. The likelihood function maximized in the unphysical region, giving a most probable signal branching fraction of $B_{Z^0 \to \mu\tau} = (-1.9^{+0.8}_{-0.6}(\text{stat})\pm0.2(\text{syst})) \times 10^{-5}$. The systematic uncertainty included the uncertainty on the efficiency, on the number of Z^0, and on the relative amount of muon pair background. The upper limit at 95% confidence level was found to be $B_{Z^0 \to \mu\tau} < 1.2 \times 10^{-5}$. This limit is stricter than previously published results. Systematic errors in the sensitivity were accounted for as discussed in section 3. It was verified that the upper limit did not increase if the background tail above 1.035 (see Fig. 3) was removed in the likelihood procedure. The stability of the results using the likelihood method with respect to the lower accepted p/E_{beam} value is demonstrated in Fig. 5.

The E_{em}/E_{beam} distribution for $e\tau$ candidates is shown in Fig. 6, for background, signal, and data. The corresponding likelihood distribution (see section 3) is shown in Fig. 7. The background was completely dominated by tau pairs. The luminosity scaled Bhabha background was 4.8 events in the whole sample, while the luminosity scaled muon pair background was estimated from simulated data to be 7.8 events. The likelihood function maximized in the unphysical region, giving a most probable signal branching fraction of $B_{Z^0 \to e\tau} = (-1.7^{+1.3}_{-1.1}(\text{stat})\pm0.3(\text{syst})) \times 10^{-5}$. The systematic uncertainty included the uncertainty on the efficiency, on the number of Z^0, and on the relative amount of Bhabha background. The 95% upper limit was found to be $B_{Z^0 \to e\tau} < 2.2 \times 10^{-5}$. Systematic errors in the sensitivity were accounted for as discussed in section 3. It was verified that the upper limit did not increase if the background tail above 1.1 (see Fig. 6) was removed in the likelihood procedure. The stability of the results using the likelihood method with respect to the lower accepted E_{em}/E_{beam} value is demonstrated in Fig. 5.

The normalized muon momentum and the normalized electron energy spectra for the $e\mu$ candidates are shown in Fig. 8 for luminosity scaled Monte Carlo simulated background and data. Fig. 9 shows the two-dimensional distribution of the electron energy versus the muon momentum for data and simulated signal. The signal region was defined by the 2σ cuts indicated by lines in the figure. Zero events passed this cut, which gave an upper limit at 95% confidence level of 0.25×10^{-5}.

7 Summary

A search for lepton flavour number violating Z^0 decays in the channels $Z^0 \to \mu\tau$, $Z^0 \to e\tau$, and $Z^0 \to e\mu$ has been performed using the DELPHI detector at LEP. The data were collected during the 1991–94 LEP runs. No signal was found. The results for the three channels are summarized in table 2. The new limits are roughly one order of

magnitude lower than the DELPHI results published previously [11]. The most optimistic realisations of the superstring inspired model with new neutral fermions [4], and of the E_6 GUT model [5], are inconsistent with these limits. The most optimistic realisations of the models of refs. [6,7] are only slightly below the limits obtained in the present work.

Acknowledgements

References

[1] M. J. S. Levine, Phys. Rev. **D36** (1987) 1329.

[2] A. Méndez and Ll. M. Mir, Phys. Rev. **D40** (1989) 251.

[3] T. K. Kuo and N. Nakagawa, Phys. Rev. **D32** (1985) 306.

[4] J. Bernabéu et al., Phys. Lett. **B187** (1987) 303.

[5] G. Eilam and T. G. Rizzo, Phys. Lett. **B188** (1987) 91.

[6] J. Bernabéu and A. Santamaría, Phys. Lett. **B197** (1987) 418.

[7] A. Ilakovac and A. Pilaftsis, Nucl. Phys. **B437** (1995) 491.

[8] M. Dittmar and J. W. F. Valle, *Flavour-changing Z decays (leptonic)*, in CERN Yellow report CERN 91–02, 1991, p.98, ed. E. Blucher, J. Jowett, F. Merrit, G. Mikenberg, J. Panman, F. M. Renard and D. Treille.

[9] E. W. N. Glover and J. J. van der Bij, *Rare Z Decays*, in CERN Yellow report CERN 89–08 Vol.2, 1989, p1, ed. G. Altarelli, R. Kleiss and C. Verzegnassi.

[10] P. Depommier and C. Leroy, Rep. Prog. Phys. **58** (1995) 61.

[11] P. Abreu et al., DELPHI Coll., Phys. Lett. **B298** (1993) 247.

[12] R. Akers et al. OPAL Coll., Z. Phys. **C67** (1995) 555.

[13] O. Adriani et al. L3 Coll., Phys. Lett. **B316** (1993) 427.

[14] D. Decamp et al. ALEPH Coll., Phys. Rep. **216** (1992) 253.

[15] P. Aarnio et al., DELPHI Coll., Nucl. Inst. Meth. **A303** (1991) 233;
P. Abreu et al., DELPHI Coll., Nucl. Inst. Meth. **A378** (1996) 57.

[16] F. A. Berends, W. Hollik and R. Kleiss, Nucl. Phys. **B304** (1988) 712.

[17] J. E. Campagne and R. Zitoun, Z. Phys. **C43** (1989) 469.

[18] S. Jadach, B. F. L. Ward, and Z. Was, Comp. Phys. Comm. **66** (1991) 276.

[19] *DELSIM: DELPHI Event Generation and Detector Simulation*, Reference Manual, DELPHI 89–68 PROG 143, 1 September 1989, unpublished.

[20] Particle Data Group, *Review of Particle Properties*, Phys. Rev. **D50** (1994), see p.1280.

[21] R. D. Cousins and V. L. Highland, Nucl. Inst. Meth. **A320** (1992) 331.

[22] P. Abreu et al., DELPHI Coll., Nucl. Phys. **B417** (1994) 3.

[23] V. Bocci et al., DELPHI trigger group, Nucl. Inst. Meth. **A362** (1995) 361;
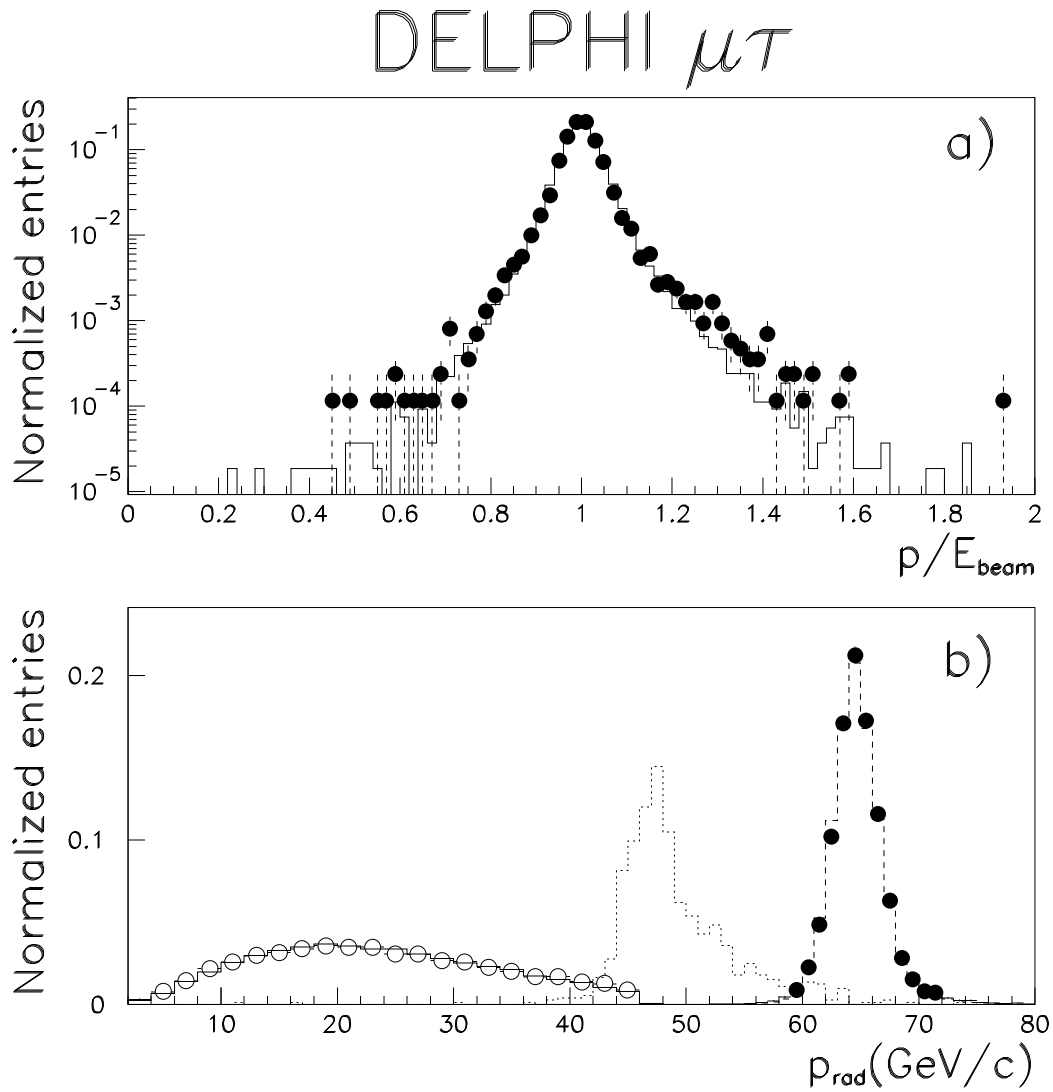P. Abreu et al., DELPHI Coll., Z. Phys. **C67** (1995) 183.

Figure 1: **a)** Muon momentum normalized to beam energy for muon pairs. Histogram is simulation, and black dots are tagged muon pairs in data. **b)** Radial momentum distributions. The dashed right histogram is Monte Carlo simulated muon pairs, black dots are tagged muon pairs in data. The left solid histogram is Monte Carlo simulated tau pairs, open circles are tagged tau pairs in data. The dotted histogram in the centre is the simulated $\mu\tau$ signal.
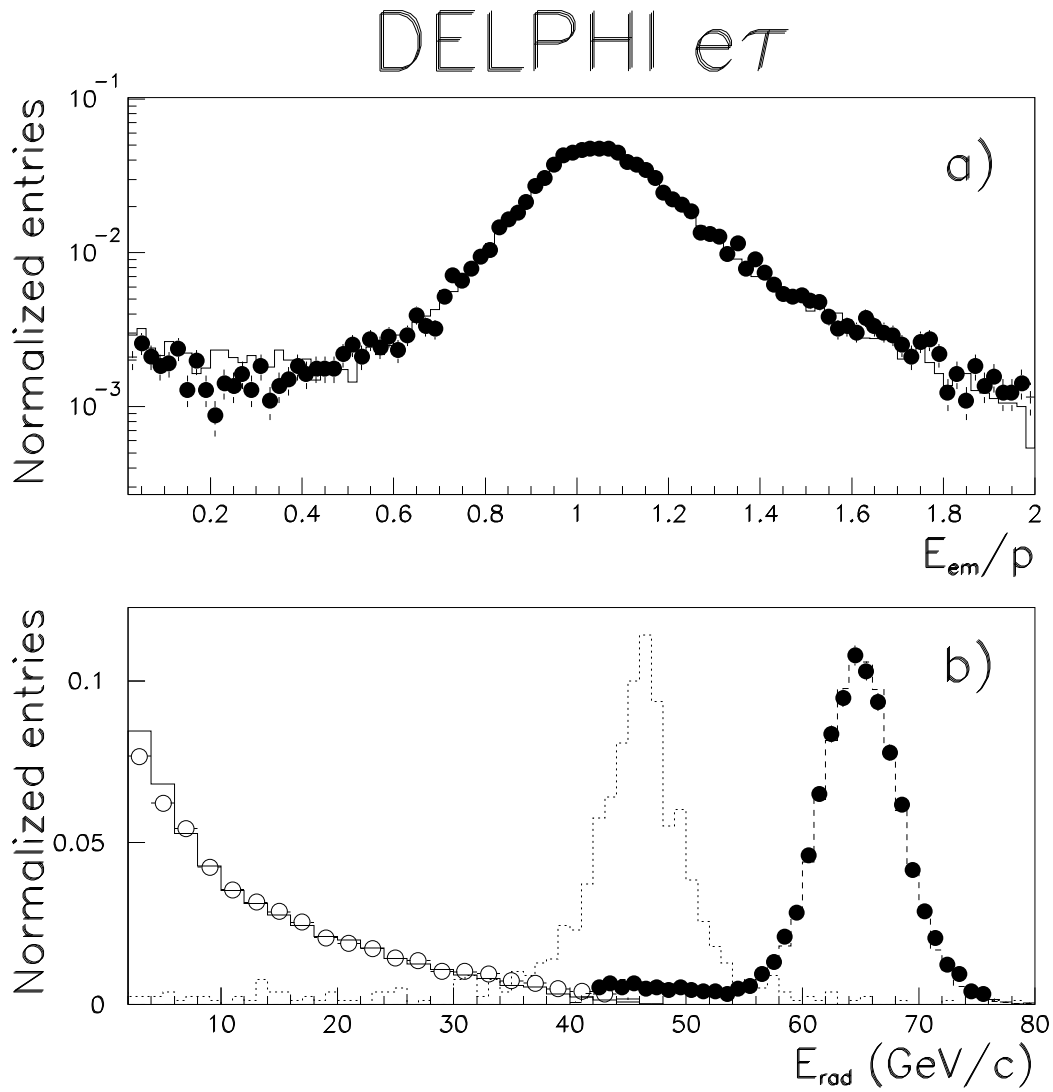
Figure 2: **a)** Electron electromagnetic energy divided by momentum for electron pairs. Histogram is Monte Carlo simulation, and black dots are tagged electron pairs in data. **b)** Radial electromagnetic energy distributions. The dashed right histogram is Monte Carlo simulated electron pairs, black dots are tagged electron pairs in data. The left solid histogram is simulated tau pairs, open circles are tagged tau pairs in data. The dotted histogram in the centre is the simulated $e\tau$ signal.
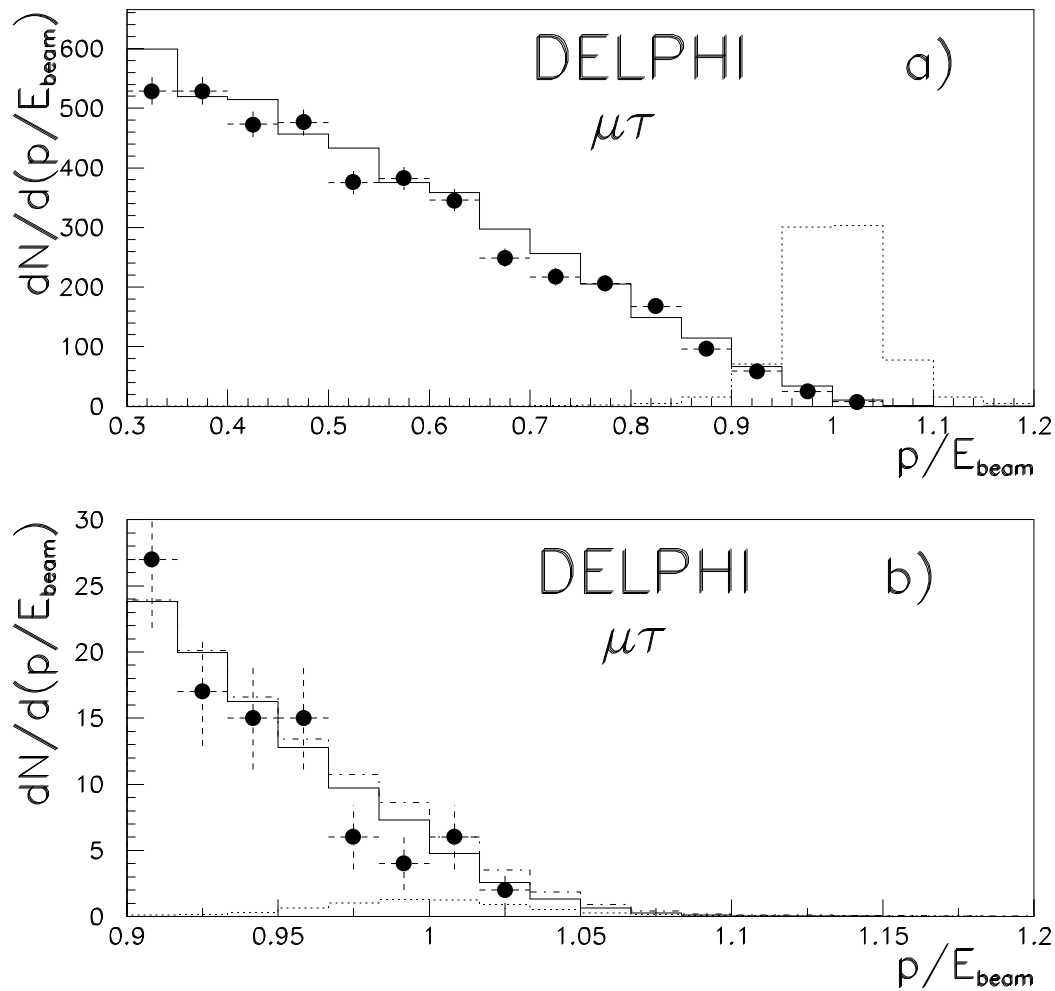
Figure 3: Normalized muon momentum spectra in $\mu\tau$ candidate events. **a)** Histogram: luminosity scaled background (from simulation). Black dots: data. Dotted histogram: signal with arbitrary normalization. **b)** The signal region. Black dots: data. Solid histogram: background corresponding to the upper limit signal fraction at 95% confidence level. Dotted histogram: signal corresponding to the upper limit. Dash-dotted histogram: background plus signal.
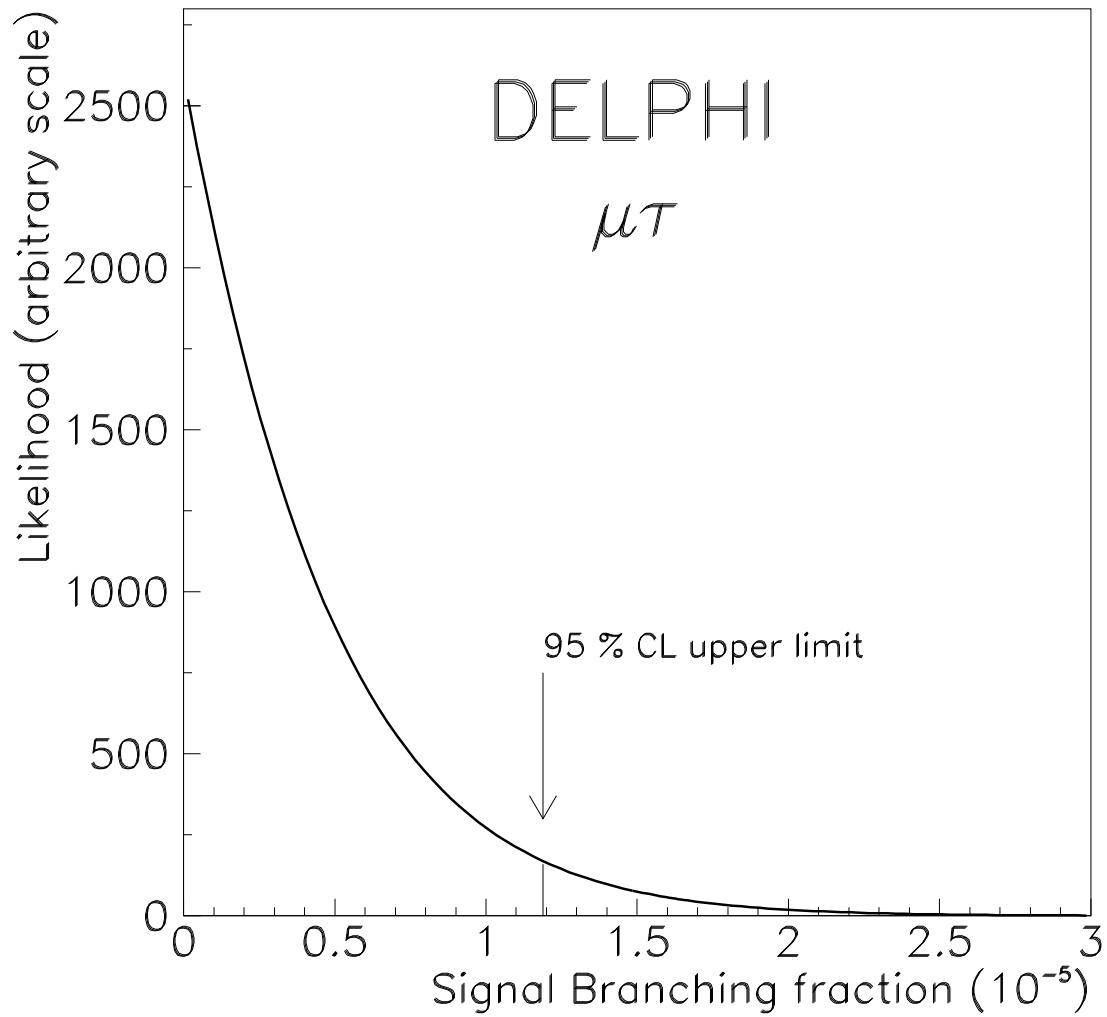
Figure 4: The likelihood as a function of the $Z^0 \to \mu\tau$ branching fraction. The upper limit at 95% confidence level is marked by a vertical line.
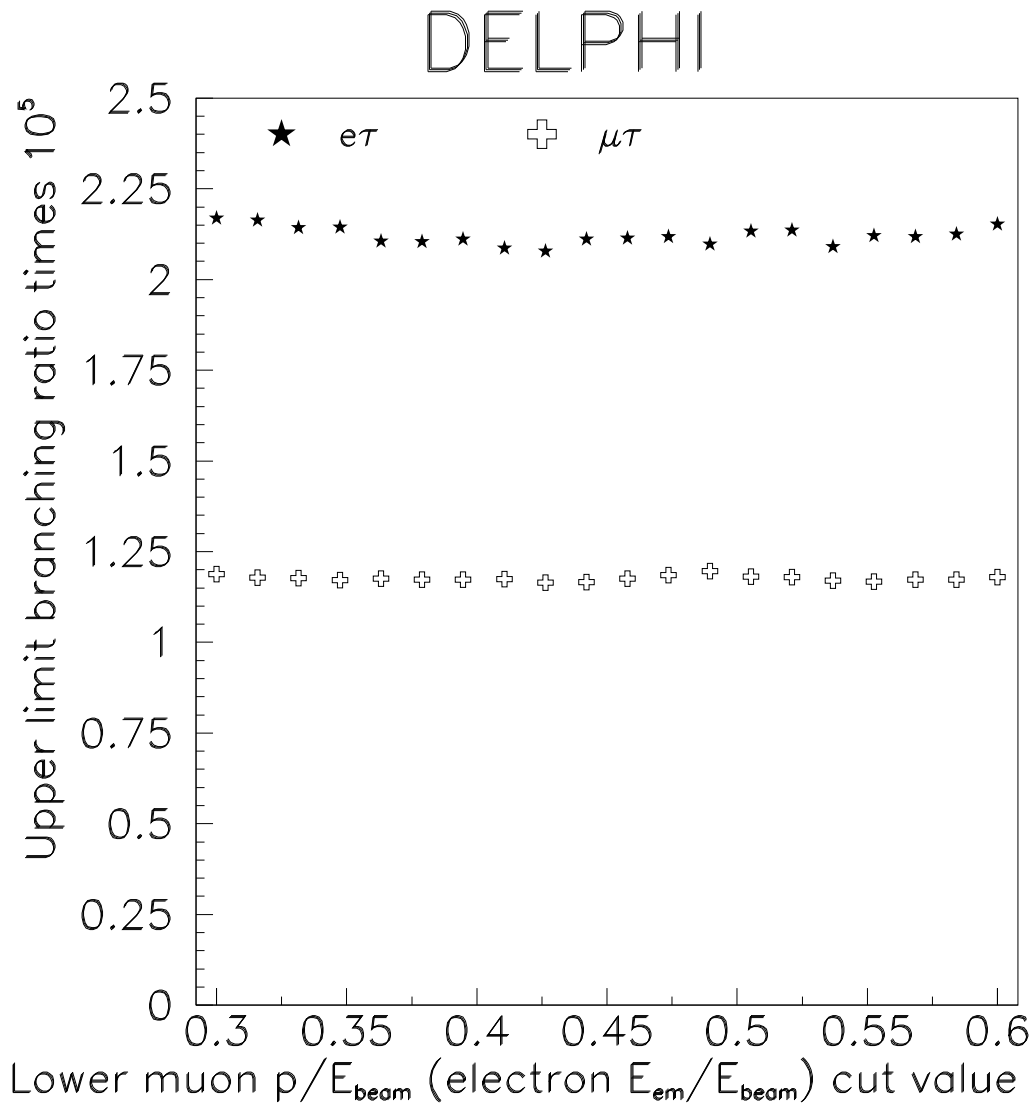
Figure 5: Signal branching fraction upper limit as a function of the lower muon p/E_{beam} (electron E_{em}/E_{beam}) cut value for the $\mu\tau$ ($e\tau$) analysis.
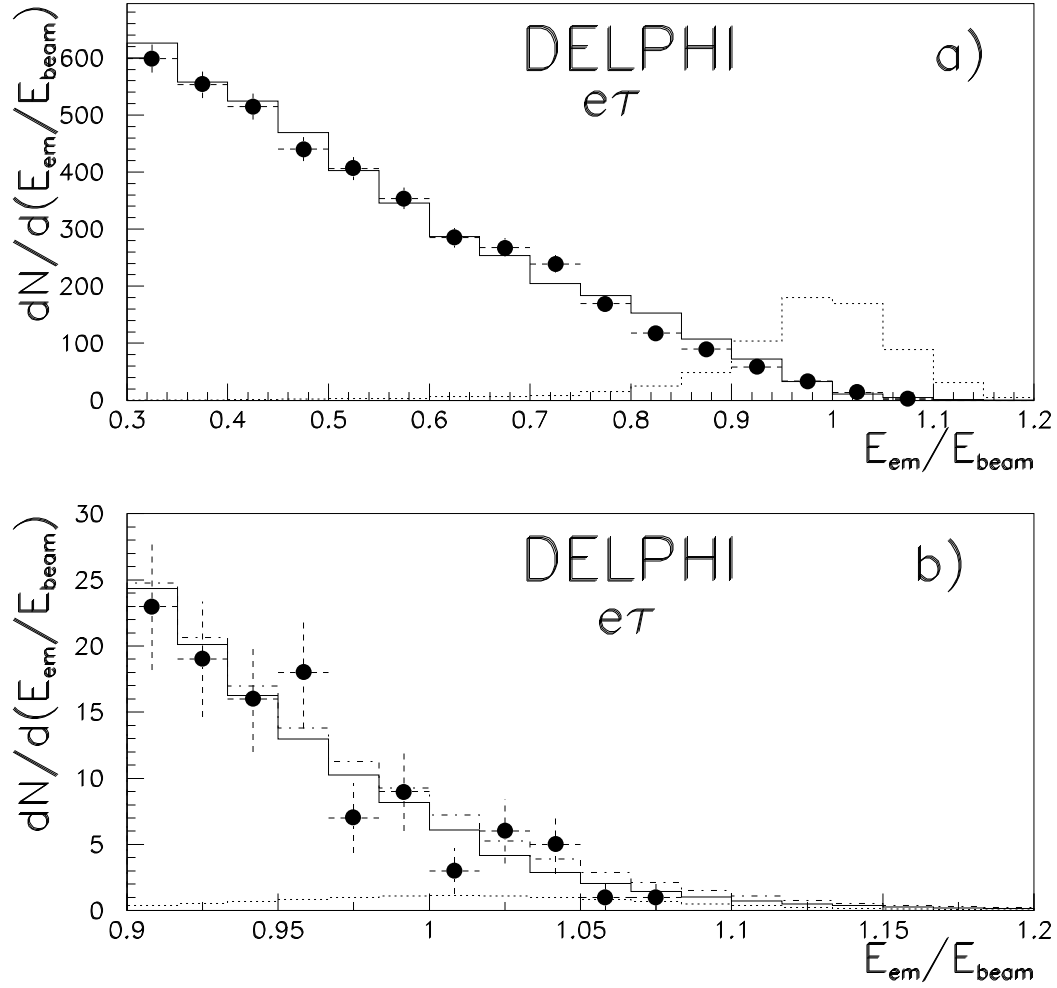
Figure 6: Normalized electron energy spectra in $e\tau$ candidate events. **a)** Histogram: luminosity scaled background (from Monte Carlo simulation). Black dots: data. Dotted histogram: signal with arbitrary normalization. **b)** The signal region. Black dots: data. Solid histogram: background corresponding to the upper limit signal fraction at 95% confidence level. Dotted histogram: signal corresponding to the upper limit. Dash-dotted histogram: background plus signal.
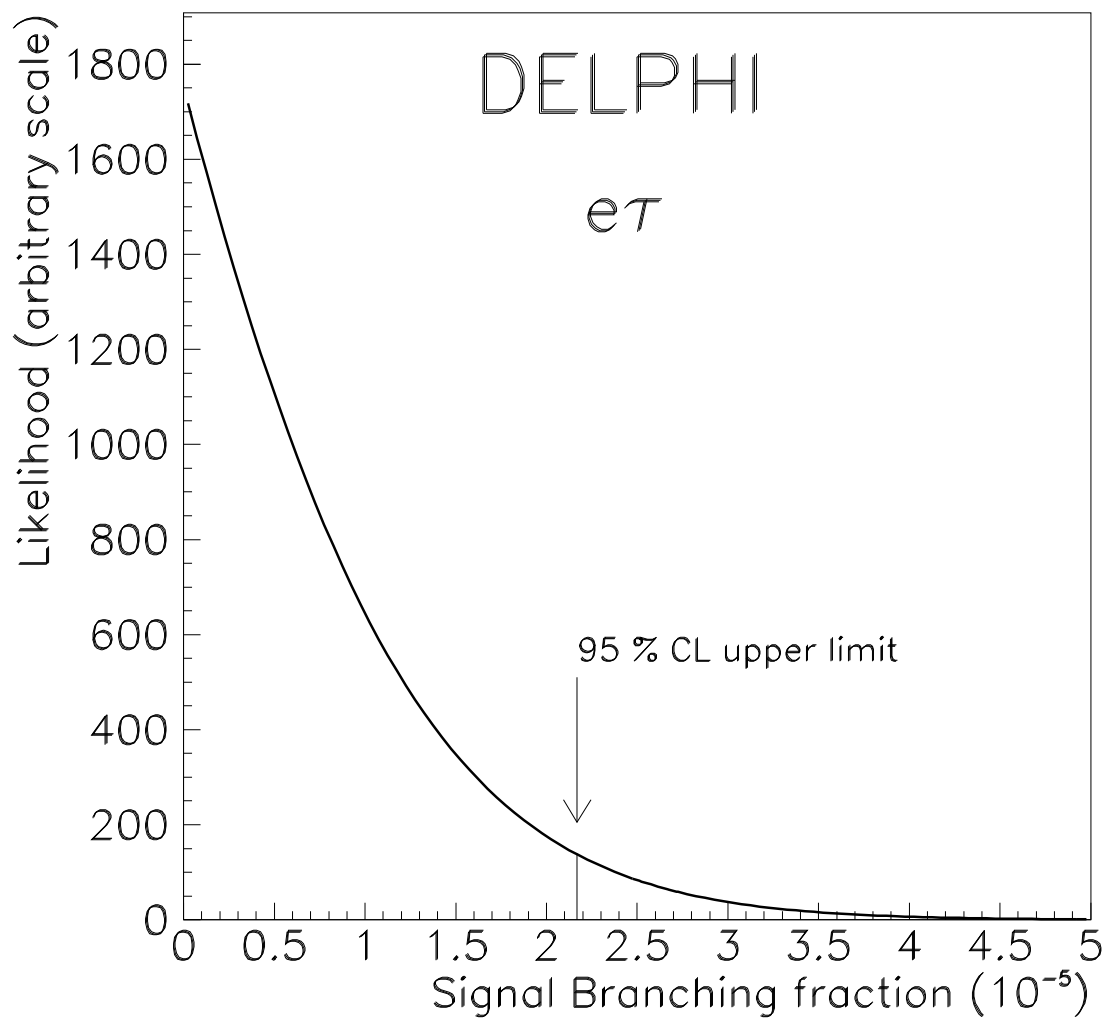
Figure 7: The likelihood as a function of the $Z^0 \to e\tau$ branching fraction. The upper limit at 95% confidence level is marked by a vertical line.
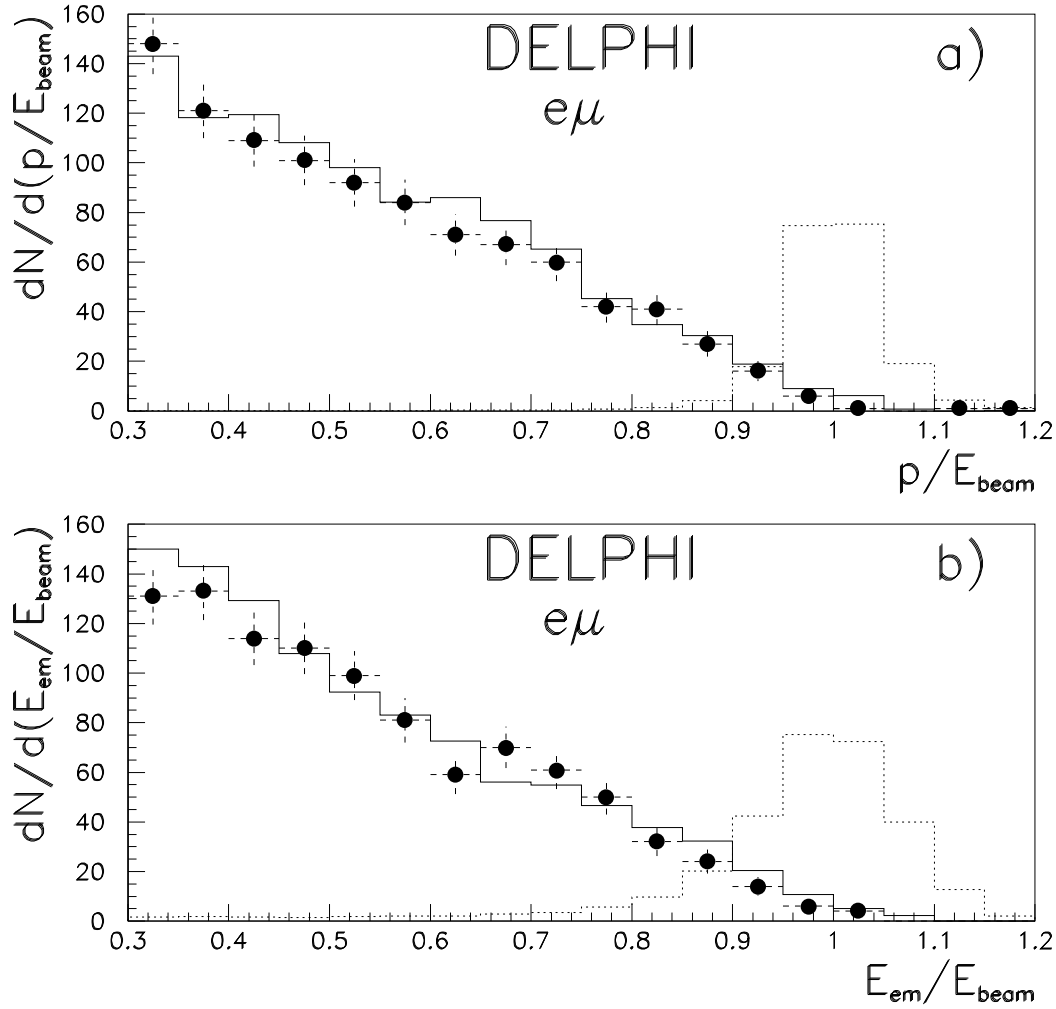
Figure 8: **a)** Normalized muon momentum for luminosity scaled Monte Carlo simulated background (solid histogram) and data (black dots) $e\mu$ candidates. Dotted histogram: signal with arbitrary normalization. **b)** Normalized electron energy for luminosity scaled Monte Carlo simulated background (solid histogram) and data (black dots) $e\mu$ candidates. Dotted histogram: signal with arbitrary normalization.
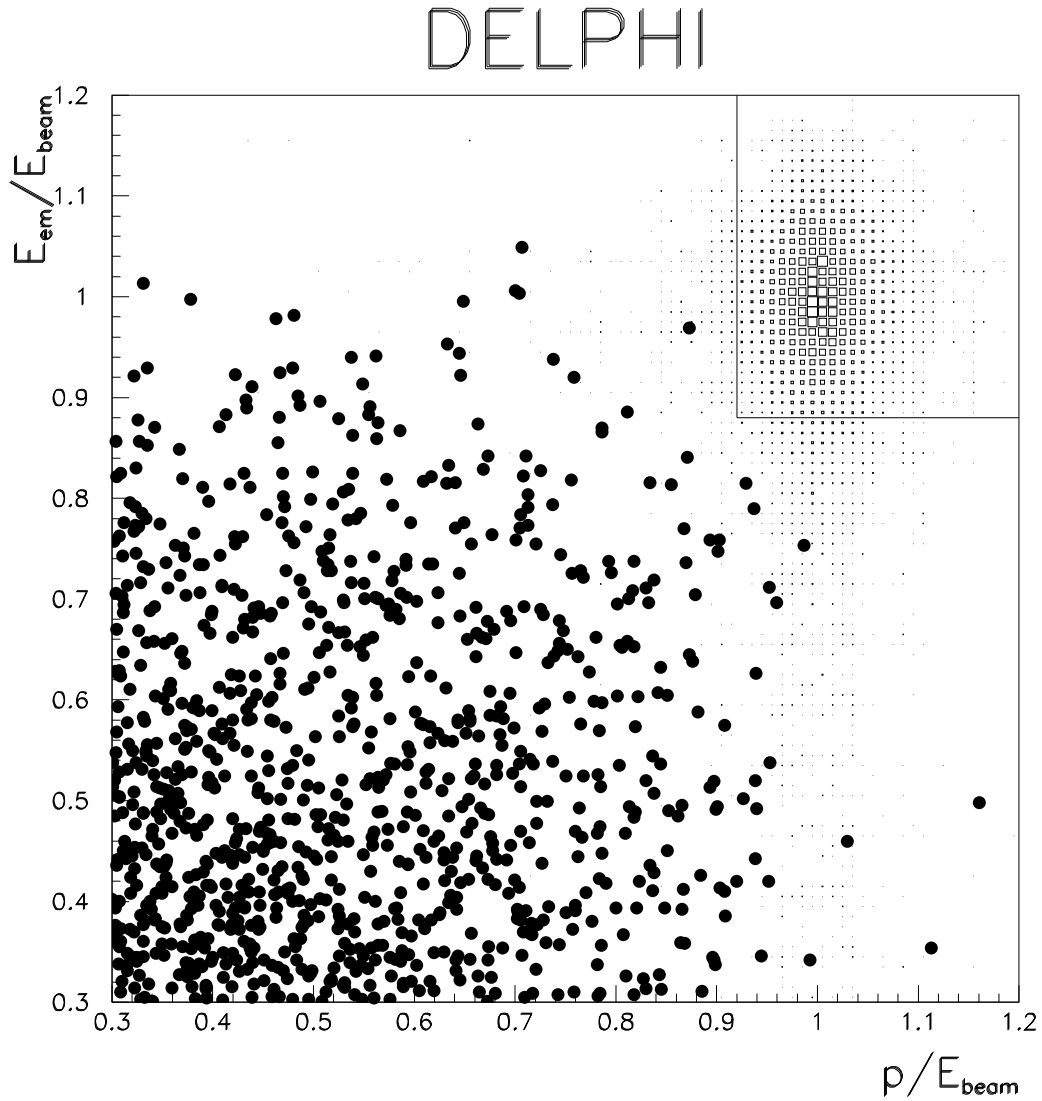
Figure 9: Normalized electron energy versus normalized muon momentum for $e\mu$ candidates. Boxes: Expected signal. Black dots: data. The area of the boxes is proportional to the number of entries in the bins. The lines define the signal region.